JACS
JOURNAL OF THE AMERICAN CHEMICAL SOCIETY
Article
Cite This: J. Am. Chem. Soc. 2019, 141, 16064−16070
pubs.acs.org/JACS

Investigating the Kinetic Competency of *Cr*HydA1 [FeFe] Hydrogenase Intermediate States via Time-Resolved Infrared Spectroscopy

Monica L. K. Sanchez,[†] Constanze Sommer,[‡] Edward Reijerse,[‡] James A. Birrell,*[,‡] Wolfgang Lubitz,*[,‡] and R. Brian Dyer*[,†]

[†]Department of Chemistry, Emory University, Atlanta, Georgia 30030, United States
[‡]Max-Planck-Institut für Chemische Energiekonversion, Stiftstrasse 34-36, 45470 Mülheim an der Ruhr, Germany

Supporting Information

ABSTRACT: Hydrogenases are metalloenzymes that catalyze the reversible oxidation of H_2. The [FeFe] hydrogenases are generally biased toward proton reduction and have high activities. Several different catalytic mechanisms have been proposed for the [FeFe] enzymes based on the identification of intermediate states in equilibrium and steady state experiments. Here, we examine the kinetic competency of these intermediate states in the [FeFe] hydrogenase from *Chlamydomonas reinhardtii* (*Cr*HydA1), using a laser-induced potential jump and time-resolved IR (TRIR) spectroscopy. A CdSe/CdS dot-in-rod (DIR) nanocrystalline semiconductor is employed as the photosensitizer and a redox mediator efficiently transfers electrons to the enzyme. A pulsed laser induces a potential jump, and TRIR spectroscopy is used to follow the population flux through each intermediate state. The results clearly establish the kinetic competency of all intermediate populations examined: H_{ox}, H_{red}, $H_{red}H^+$, $H_{sred}H^+$, and H_{hyd}. Additionally, a new short-lived intermediate species with a CO peak at 1896 cm^{-1} was identified. These results establish a kinetics framework for understanding the catalytic mechanism of [FeFe] hydrogenases.

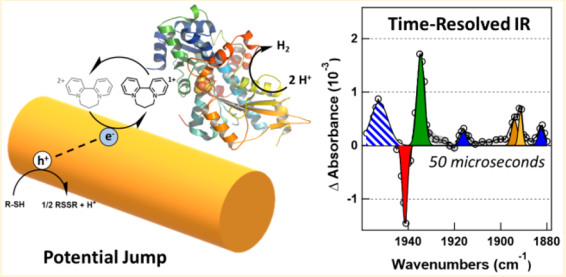

INTRODUCTION

Hydrogenases catalyze the reversible cleavage of H_2 with high turnover frequency and minimal overpotential, using earth abundant transition metals.[1] These highly efficient enzymes have inspired chemists for decades in an effort both to understand their mechanisms and to reproduce their chemistry in biomimetic systems.[2−9] [FeFe] hydrogenases are particularly interesting because of their high activity, especially in hydrogen production.[1,6,10] For these reasons, numerous studies have probed the catalytic cycle of [FeFe] hydrogenases, including extensive pH-dependent FTIR spectroelectrochemical experiments.[11−14] These studies have led to the identification of a series of resting states of the H-cluster differing by one or two electrons, or one proton, or both.[11,15] Although it is tempting to align these states as intermediates in a catalytic cycle,[11−13,15] questions remain whether all of these states are on pathway and whether other short-lived intermediates are involved that cannot be stabilized as resting states. Furthermore, several different catalytic cycles have been proposed, involving distinct ET/PT intermediates, some involving stepwise ET/PT with variations in the ordering of the steps[11,12,15,16] and others involving concerted PCET[13,17] (Figure 1). Therefore, a detailed kinetics investigation of each of the intermediate states proposed to be catalytically relevant is critical to building a comprehensive catalytic model of [FeFe] hydrogenases. Capturing these intermediate states kinetically has proven challenging, however, due to the very rapid turnover rate of [FeFe] hydrogenases.

In this study, we employ a laser-induced potential jump coupled with time-resolved infrared (TRIR) spectroscopy to study the catalytic mechanism of the [FeFe] hydrogenase from *Chlamydomonas reinhardtii* (*Cr*HydA1). This methodology was previously demonstrated to be capable of following the time-dependent population of hydrogenase intermediates on subturnover time scales.[18,19] Using this approach, we address the critical questions of which intermediates are kinetically competent to be part of the catalytic cycle and determine the flux through each state during turnover of *Cr*HydA1. The results presented here provide a framework for addressing which intermediates are significantly populated as part of the catalytic cycle, by (a) identifying distinct transient spectroscopic signatures for all relevant intermediate states, such that the kinetics of each can be probed on subturnover time scales; (b) demonstrating the kinetic competency of all of these states; and (c) identifying the critical rate-determining step (RDS) of the catalytic cycle.

Received: August 2, 2019
Published: September 11, 2019

DOI: 10.1021/jacs.9b08348
J. Am. Chem. Soc. 2019, 141, 16064−16070

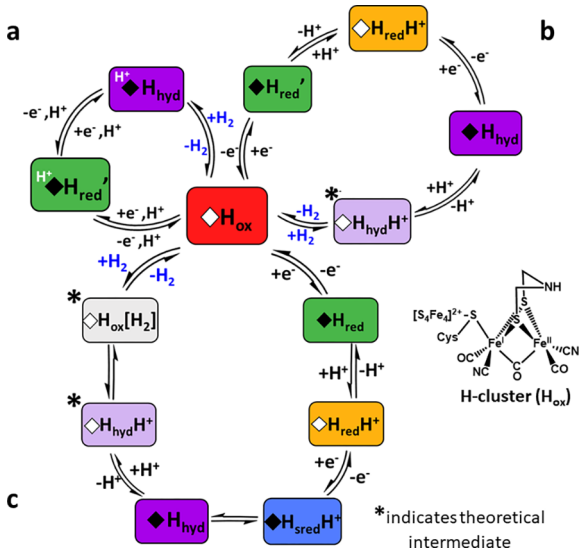

Figure 1. Scheme relating simplified versions of three recently proposed catalytic cycles for *Cr*HydA1 [FeFe] hydrogenase. (a) Adapted from ref 17. (b) Adapted from ref 15 (simplified to show only main pathway for *Cr*). (c) Adapted from ref 11. ♦ = $[Fe_4S_4]^{1+}$ cluster; ◊ = $[Fe_4S_4]^{2+}$ cluster. Colored rectangles indicate different H-cluster intermediate states identified in steady state measurements: Red = oxidized; green = 1 e^- reduced; yellow = 1 e^- and 1 H^+; blue = 2 e^- and 1 H^+; purple = hydride; light purple = hydride and 1 H^+; * = postulated intermediate. H_{hyd} and $H_{hyd}H^+$ labels refer to the same state and reflect literature variations in the nomenclature.

EXPERIMENTAL SECTION

Hydrogenase Sample Preparation. *Cr*HydA1 was prepared as previously described.[20] Samples were prepared anaerobically in a glovebox with 5% H_2 in a N_2 atmosphere. A 4 mM stock solution of *Cr*HydA1 hydrogenase was exchanged into 50 mM potassium phosphate, 50 mM mercaptopropionic acid (MPA) at pH = 8.4 buffer solution by several 1:5 dilution steps followed by concentration using a 10 kDa molecular weight cutoff filter (EMD Millipore). The sample was then transferred to a septum sealed glass vial where it was mixed with 10 μL of a stock solution of CdSe/CdS nanorods and 2 μL of a 0.5 M stock solution of 2,2′-propylbipyridinium (DQ03) mediator. After buffer exchange and addition of photosensitizer and mediator, the final protein concentration was 2.5 mM. The sample was then loaded into one side of a two compartment, airtight FTIR cell via gastight syringe. The FTIR cell consisted of two CaF_2 windows mounted in a copper holder with a 50 μm thick Teflon spacer divided into two compartments. The other compartment contained the reference which had been prepared identically to the hydrogenase sample except with deoxymyoglobin (deoxyMb) instead of hydrogenase. The reference solution concentration was adjusted to match the optical density of the sample absorbance at 355 nm. The FTIR sample was then incubated under N_2 for 24 h prior to experiments to allow any H_2 trapped in the cell to diffuse out of the cell.

Fourier Transform Infrared (FTIR) Spectroscopy. FTIR spectra of hydrogenase samples used for transient measurements were obtained with a Varian 660 FTIR spectrometer equipped with a liquid nitrogen cooled MCT detector. Reported spectra represent the average of 2048 scans at 2 cm^{-1} resolution and were baseline corrected with a multipoint spline function. A difference FTIR spectrum was computed from the single beam spectra obtained in the dark (I_{dark}) and after laser illumination (I_{light}) to determine the degree of photoreduction of the hydrogenase. The "dark" spectrum was obtained for a sample containing protein, nanorods, and mediator that was kept in the dark, whereas the "light" spectrum was obtained by illuminating the same sample with a diode laser at 405 nm (4 mW focused to a 1 mm spot) for 10 s and then collecting the single beam spectrum. Difference spectra were computed as $\Delta A(bs) = -\log(I_{light}/I_{dark})$.

Simultaneous Transient Visible/Infrared Absorption Spectroscopy. Nanosecond transient absorbance was used to follow the generation of reduced mediator ($DQ03^{+\bullet}$, 785 nm), its consumption by the enzyme and the concomitant response of the H-cluster (CO absorbance near 5 μm). The instrument used to collect the nanosecond TRIR and visible transient absorbance (TA) data simultaneously has been described previously.[19] Briefly, the pump−probe experiment employs the third harmonic of a Q-switched Nd:YAG laser (10 ns pulse at 355 nm) as the pump pulse and two continuous wave probe lasers, a QCL operating in the mid-IR and a 785 nm diode laser. The time-resolved absorbance of the two probe beams is detected using a fast MCT detector and an avalanche photodiode, respectively. Single shot transients were collected at room temperature using 100 μJ of 355 nm light focused to an ~500 μm diameter spot (50 mJ/cm^2). The sample position was shifted to ensure a new sample volume was probed with each laser shot. An average of 20−25 shots was obtained for every probe wavelength. The transient absorbance signal was calculated as $\Delta A = -\log(I_{light}/I_{dark})$, where I_{dark} is the signal before the arrival of the pump pulse at time zero. The pump pulse slightly heats the water (1−2 °C temperature jump due to nonradiative relaxation of excess pump energy), producing a transient IR background signal (due to the temperature dependence of the mid-IR water absorbance) that rises within 10 ns and decays on the 1 ms time scale.[21] An identical water background signal was produced by the deoxyMb reference and subtracted from the sample transient to yield the corrected ΔA response of the hydrogenase.

Data Analysis. The IR transients were fit using IGOR software (Wavemetrics, Inc.) to multiexponential fit functions. The time-resolved IR spectra were fit to multiple Gaussian peaks using IGOR software with a global fitting procedure.

RESULTS AND DISCUSSION

Rapid Initiation of Hydrogenase Turnover Using a Potential Jump. In previous work, we established an approach to photoinitiate turnover of a hydrogenase using a photosensitizer and electron carrier to produce a potential jump on the subturnover time scale.[19,22,23] Here, we have applied this technique to study the mechanism of *Cr*HydA1 [FeFe] hydrogenase. All experiments were performed at pH = 8.4 because the rods are more stable and the yield of reduced mediator is optimized at this pH. We employed a nanocrystalline semiconductor CdSe/CdS dot-in-rod (DIR) as the photosensitizer and a propyl bridged 2,2′-bipyridinium (DQ03) as the electron carrier (Figure 2A).[24,25] Coupling this phototriggering method with nanosecond time-resolved infrared (TRIR) spectroscopy yields a powerful tool to monitor the chemistry occurring at the active site.[19] Upon pulsed laser excitation of the DIR photosensitizer, an electron is promoted to the conduction band, followed by ET to the mediator LUMO (Figure 2B). This ET step occurs with near-unity quantum efficiency[26] and results in a rapid (~10 ns) potential jump as the solution potential becomes more negative by 400−500 millivolts, triggering turnover via ET to the enzyme.

The magnitude of the change in solution potential and the rate of ET to the enzyme were determined with visible transient absorption (TA) spectroscopy by monitoring the DQ03 chromophore. The reduced redox mediator, $DQ03^{\bullet+}$, has a strong and broad absorption band in the red spectral region, whereas the oxidized mediator $DQ03^{2+}$ does not absorb in this region.[26] Thus, the production of the reduced mediator and subsequent ET to the enzyme was monitored with TA probing at 785 nm and the change in solution potential is calculated using the Nernst equation (Supporting Information (SI)). The relative time scales and energy levels of these ET events are depicted in the diagram in Figure 2B.

DOI: 10.1021/jacs.9b08348
J. Am. Chem. Soc. 2019, 141, 16064−16070

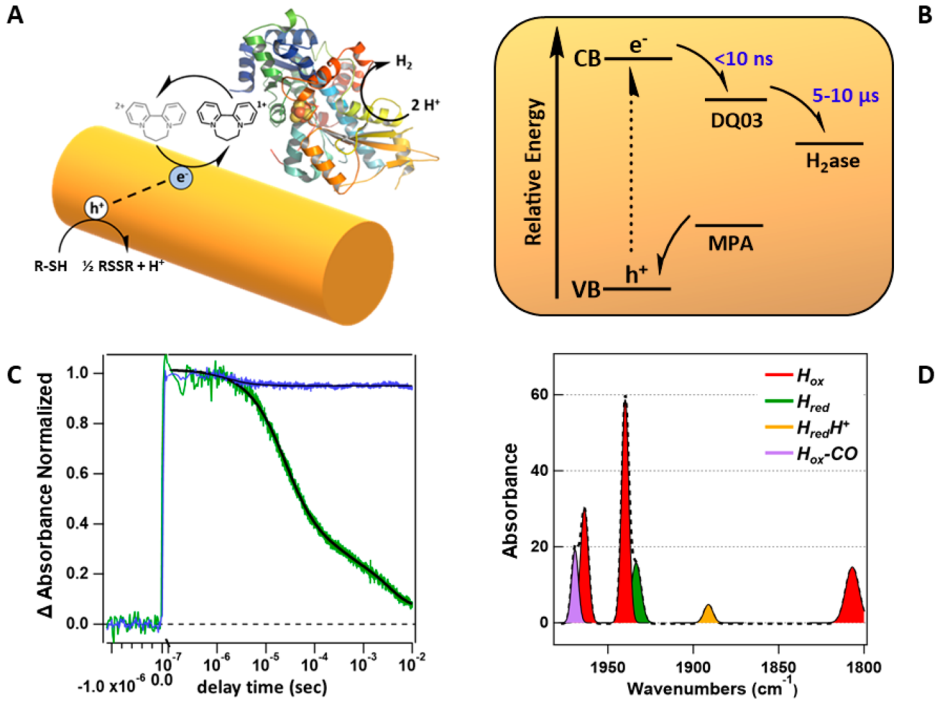

Figure 2. Laser-induced potential jump. (A) Electron transport pathway: light absorption generates exciton in CdSe/CdS nanorod, followed by reduction of DQ03 mediator and ET to *Cr*HydA1 (crystal structure of apo-*Cr*HydA1 adapted from ref 23, PDB 3LX4). (B) Energy diagram depicting the relative energy level and rates (ref 19) of each ET step; MPA = mercaptopropionic acid, present as the DIR capping ligand and acting as the sacrificial electron donor; h^+ = hole remaining in the valence band (VB) of the material. (C) Potential jump monitored by transient absorbance (TA) of the radical at 785 nm for the HydA1 sample (green) compared to the deoxyMb (blue) reference. (D) Representative FTIR spectrum of the *Cr*HydA1 sample used for laser-induced potential jump measurements. Intermediate populations are colored as follows: Mauve = H_{ox}–CO, Red = H_{ox}, Green = H_{red}, Gold = $H_{red}H^+$.

Two samples were compared, both containing the same concentrations of DQ03 and DIR but differing in whether they contained either *Cr*HydA1 or a reference protein, deoxyMb. The absorbance of the deoxyMb reference at 355 nm is matched to that of the hydrogenase sample to account for any inner filter effects of the protein absorbance. Representative 785 nm absorption transients for the *Cr*HydA1 and deoxyMb samples are compared in Figure 2C. In both samples, the 785 nm absorption signal due to $DQ03^{+\bullet}$ radical formation rises with an instrument limited lifetime of <10 ns. The concentration of radical produced was between 400 and 500 μM on average depending on pump power. The rate of ultrafast reduction of $DQ03^{2+}$ by the DIR photosensitizer has been well-established[26,27] and agrees well with the results of this control experiment. The deoxyMb reference transient features a small amplitude single exponential decay of radical population with a lifetime of 16 μs. This initial decay is due to charge recombination, i.e. back electron transfer from the radical to the remaining hole in the DIR; this process is inefficient because it competes with hole quenching by the thiolate sacrificial electron donor. After this small initial decay, the TA signal remains constant out to tens of ms, indicating the stability of the reduced mediator in the absence of an electron acceptor. In contrast, a multiexponential decay of the 785 nm radical absorption is observed for the hydrogenase sample. Most of the decay (~65%) occurs in two initial phases with lifetimes of 16 and 61 μs, indicating that the bulk of the enzyme is reduced on this time scale. A slightly slower phase with a lifetime of 291 μs (25%) is also observed, meaning ~90% of the radical is consumed on a time scale that is faster than the turnover time (~2 ms) previously found for this enzyme.[8] We also measured the steady state turnover rate of the enzyme under the potential jump conditions (pH 8.4, nanorod photosensitizer, mediator). Continuous illumination generates a steady state population of reduced mediator, which in turn causes steady state turnover of the enzyme. The steady state rate we observe under these conditions (900 s^{-1}) is slightly faster than what was reported previously, but still consistent with the potential jump results.

Photoprotection of the Enzyme by the Photosensitizer. Several groups have observed degradation of [FeFe] hydrogenase samples after some period of light exposure.[28,29] The observed product of degraded protein is a CO inhibited H-cluster, termed H_{ox}–CO, resulting from the release of the intrinsic carbonyl ligands from degraded H-clusters that are subsequently captured by intact H-clusters.[29−31] H_{ox}–CO has been well characterized and features an oxidized H-cluster with the additional CO bound in a terminal position on the distal Fe.[32−34] We tested the photostability of *Cr*HydA1 during the course of the experiments by measuring the FTIR spectrum before and after data collection. Based on the FTIR spectra collected (Figure 2D), we consistently found <10% growth of the H_{ox}–CO population under the conditions of our potential jump experiments. We attribute the photostability of the enzyme in these experiments to the high extinction coefficient of the CdSe/CdS nanorods (>100,000 M^{-1} cm^{-1})[35] compared to that of the enzyme (~35 000 M^{-1} cm^{-1}) at the pump wavelength. Apparently, the strongly absorbing rods protect the enzyme from light damage.

Potential jump experiments on the CO-inhibited enzyme provide further support for the photoprotection of the enzyme by the photosensitizer (SI). They also demonstrate the importance of careful selection of the probe frequency to

DOI: 10.1021/jacs.9b08348
J. Am. Chem. Soc. 2019, 141, 16064−16070

avoid overlapping absorbances of multiple species. For example, a probe frequency of 1954 cm^{-1} should report on both the H_{red}–CO and the $H_{sred}H^+$ intermediates, but the transient at this frequency in Figure S4 is clearly dominated by the rise of the H_{red}–CO absorbance. The unique $H_{sred}H^+$ absorbance at 1882 cm^{-1} gives a very different transient response, corresponding to the slower conversion of H_{red}–CO to $H_{sred}H^+$. The presence of any CO inhibited enzyme in the sample has the potential to obscure the detection of this and other catalytic intermediates. Therefore, we selected probe frequencies corresponding to unique CO absorptions not overlapped with other states to follow the subturnover kinetics of the intermediate states of the H-cluster.

H-cluster Subturnover Kinetics at pH 8.4. The TA results indicate that *Cr*HydA1 is reduced on a subturnover time scale by the laser-induced potential jump. Consequently, all of the intermediate states of the H-cluster can be probed by TRIR spectroscopy on this same time scale using their unique infrared signatures. Figure 3 shows frequency-dependent TRIR transients for *Cr*HydA1 following a laser-induced potential jump. Specific IR frequencies were selected to follow the kinetics of formation or loss of a specific intermediate state based on previous assignments of the IR spectra (Figure S2).[11] Only CO frequencies were investigated because these give larger signals and better resolution for individual states compared to the CN^-

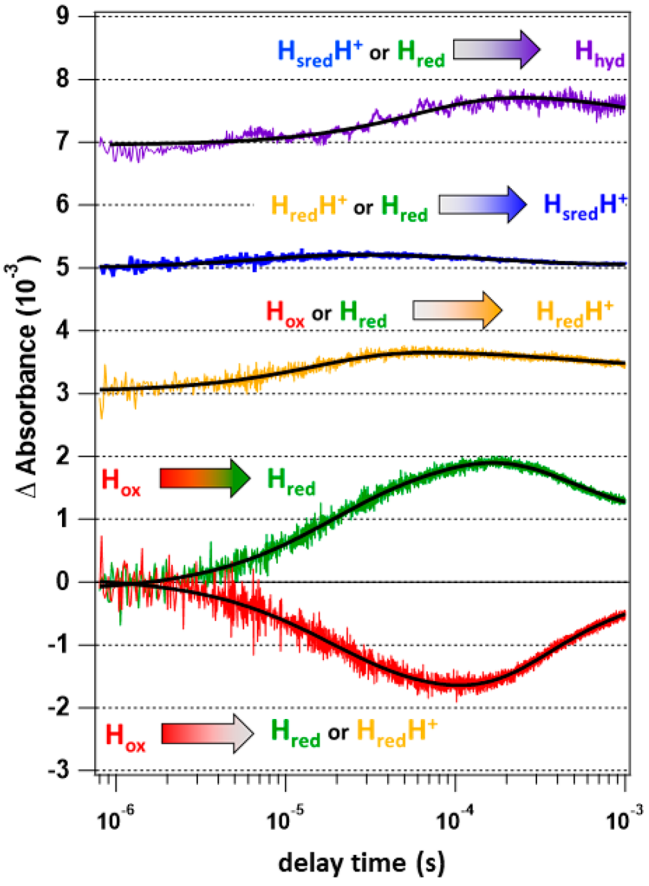

Figure 3. H-cluster kinetics. (Red) H_{ox} kinetics monitored at 1941 cm^{-1}; (Green) H_{red} kinetics (1 e- reduced state) at 1934 cm^{-1}; (Gold) $H_{red}H^+$ kinetics at 1891 cm^{-1}; (Blue) $H_{sred}H^+$ kinetics (2 e- reduced state) at 1882 cm^{-1}; (Purple) H_{hyd} kinetics at 1859 cm^{-1}. The indicated transitions correspond to the initial bleach or rise of each transient. The black lines represent multiexponential fits as described in the text.

bands. The enzyme sample as prepared was initially in a mixed oxidation state, with the majority being in H_{ox}, but also a significant population (~35%) of the one-electron reduced states H_{red} and $H_{red}H^+$. A substoichiometric amount of reduced mediator is produced by the potential jump (approximately a 1:5 ratio of reduced mediator to enzyme), meaning on average each enzyme receives less than a single electron. Consequently, the potential jump is insufficient to carry the population of enzyme that is initially in the oxidized state completely through the catalytic cycle, since this requires two electrons. Nevertheless, the potential jump results in complete cycling of some population of the enzyme, since some one-electron reduced enzyme is present initially. Thus, it is possible to track the population flux through all intermediate states in the potential jump experiment, although the resulting kinetics are complex.

H_{ox} Kinetics (1941 cm^{-1}). The rates of H_{ox} depletion and recovery establish the end points of the catalytic cycle (Figure 3): the bleach of the H_{ox} absorbance at 1941 cm^{-1} corresponds to the initial one-electron reduction of the enzyme, starting the catalytic cycle, and the recovery of the bleach corresponds to regeneration of H_{ox} at the end of the catalytic cycle. The bleach is modeled by a biexponential function with lifetimes of 14 μs (35%) and 75 μs (65%). These lifetimes are the same as those observed for the consumption of the reduced mediator $DQ03^{+\bullet}$ (16 and 61 μs) within the error of the measurement (SI Table S2), meaning there is no observable delay between oxidation of the mediator and reduction of the H-cluster as expected for direct outer sphere ET from the mediator to the H-cluster. The two observed rates may be due to two different ET pathways into the enzyme. The native redox partner, photosynthetic electron transfer ferredoxin (PetF), forms a highly specific ET complex with *Cr*HydA1, but this is not likely the case for the polypyridyl mediator employed here. Furthermore, there are no auxiliary FeS clusters that define a specific ET pathway in this hydrogenase, unlike for instance hydrogenases from *Desulfovibrio desulfuricans* or *Clostridium acetobutylicum*.[1,13,15,36] Thus, it is not surprising that we observe multiple rates for reduction of H_{ox} by the mediator. At longer times, the recovery of the 1941 cm^{-1} bleach corresponds to the turnover of the enzyme, which regenerates the H_{ox} state. A biexponential recovery is observed with lifetimes of 180 μs (65%) and 900 μs (35%). The 180 μs component is significantly faster than the turnover lifetime (900 s^{-1} under the potential jump conditions or 1.1 ms lifetime), meaning it is likely to arise from some other process. We tentatively attribute this fast recovery of the H_{ox} population to disproportionation of H_{red} to yield H_{ox} and $H_{sred}H^+$. The 900 μs component is slightly faster than what is predicted from the steady state turnover rate (1.1 ms). Apparently, the final chemical step that regenerates H_{ox} is not rate-determining, meaning the steady state kinetics must be limited by some other process such as hydrogen diffusion out of the protein.

H_{red} Kinetics (1934 cm^{-1}). The production of H_{red} is monitored by the transient absorbance at 1934 cm^{-1}, which has two main components with lifetimes of 12 and 61 μs. The close correspondence of these lifetimes with those due to H_{ox} depletion is consistent with direct, one-electron reduction of H_{ox} to produce H_{red}. The H_{red} transient absorbance does not recover to baseline, because the potential jump generates a substoichiometric number of reducing equivalents and further progress through the cycle requires two electrons. The competing pathway of one-electron reduction of the initial population of H_{red} (presumably to form $H_{sred}H^+$) should cause a decrease in the absorbance at 1934 cm^{-1}; such a decrease is observed at

DOI: 10.1021/jacs.9b08348
J. Am. Chem. Soc. 2019, 141, 16064–16070

longer times, with a lifetime of 525 μs, well within the turnover lifetime. A faster phase of H_{red} reduction is likely present based on the observed fast formation of $H_{sred}H^+$ (see below), but this phase is opposite in sign and therefore obscured by the rapid rise in H_{red} caused by reduction of H_{ox}. In summary, the observed reduction of H_{red} is significantly slower than H_{ox} but still within the lifetime of the catalytic cycle.

$H_{red}H^+$ Kinetics (1891 cm^{-1}). A single exponential rise with a lifetime of 15 μs is observed at 1891 cm^{-1}, corresponding to a fast one-electron reduction of H_{ox} to produce $H_{red}H^+$. The production of $H_{red}H^+$ occurs with the same lifetime as the fast reduction of H_{ox}. These observations are consistent with a concerted ET/PT process that directly converts H_{ox} to $H_{red}H^+$. It is not clear why the slower (75 μs) rate of reduction of H_{ox} does not have a corresponding rise in the $H_{red}H^+$ transient. Since formation of H_{red} from H_{ox} is an ET process, whereas formation of $H_{red}H^+$ involves PCET, their nearly identical formation rates means that the PT step that forms $H_{red}H^+$ is fast and thus the ET and PCET processes occur at similar rates. It also means that the ET and PCET processes are occurring in parallel, probably because at pH 8.4 the proton donor for the PCET process is only partially protonated. The decay of the 1891 cm^{-1} absorbance is observed with a lifetime of 540 μs. Some $H_{red}H^+$ is initially present in the sample, and its decay corresponds to a second one-electron reduction of the enzyme.

$H_{sred}H^+$ Kinetics (1882 cm^{-1}). This state is formed very rapidly, with a 7 μs rise and decays within 210 μs. The rapid rise of this state should have a corresponding depletion of the H_{red} or $H_{red}H^+$ state, but this is not observed, perhaps because it is obscured by rapid production of these states from H_{ox}, which is the dominant process in the potential jump with the present conditions. Nevertheless, it is clear this state is produced and decays well within the lifetime of the catalytic cycle.

H_{hyd} Kinetics (1859 cm^{-1}). The H_{hyd} state shows a fast rise with a lifetime of 60 μs and slow decay on the order of 1 ms. The formation lifetime of H_{hyd} is consistent with its origin being the $H_{sred}H^+$ state, because the latter decays on a similar time scale to the H_{hyd} rise, although we cannot rule out direct conversion of H_{red} or $H_{red}H^+$ to H_{hyd}. Thus, the present results confirm that $H_{sred}H^+$, $H_{red}H^+$, and H_{red} are each kinetically competent to form H_{hyd}. The decay of the H_{hyd} state is on the same time scale as the recovery of the H_{ox} state and therefore corresponds to completion of the catalytic cycle. The 1859 cm^{-1} transient shows a small negative baseline offset at $t < 5$ μs due to imperfect subtraction of the temperature-dependent background absorbance of water (by the procedure outlined in Figure S3). This baseline offset is easily distinguished from the protein signal due to its distinct time dependence (it rises on the nanoscale time scale of the instrument response), and it does not influence the fit of the protein signal.

TRIR spectra reveal a new intermediate state. The kinetics experiments described above only probe intermediate states observed previously in equilibrium or steady state kinetics experiments. The question remains whether there are additional intermediates that have not been detected in steady state measurements due to their short lifetimes. For example, the protonation of H_{hyd} to form H_2 at the active site, presumably coordinated to the distal Fe, has never been observed. We searched for possible new intermediate states by measuring the complete time-resolved IR spectrum at subturnover times in the carbonyl stretching region (1880−1958 cm^{-1}), in response to a laser-induced potential jump. All known *Cr*HydA1 intermediate states have CO bands in this region, so this is a reasonable starting range to search.[13,17,37] TRIR kinetics were measured from 100 ns to 10 ms stepwise at probe frequencies spaced by 1−2 cm^{-1} over this spectral range in order to generate TRIR spectra (Figure 4). Multiple (>10) IR transients were collected at each probe frequency and averaged. Figure 4A shows the IR transients collected at IR frequencies (1891, 1893, 1895 cm^{-1}) near the CO band of the $H_{red}H^+$ intermediate. Time-resolved IR spectra are obtained as "time slices" through the IR transients, by plotting the ΔA at a specific time-delay versus wavenumber (cm^{-1}) as shown in Figure 4B. The TRIR spectra are then fit to Gaussian line shapes with a global fitting procedure. Figure 4 compares the TRIR spectra at progressively longer delays to the steady-state FTIR difference spectrum obtained by subtracting the spectrum in the dark from a spectrum following continuous illumination to generate a steady-state population of reduced enzyme.

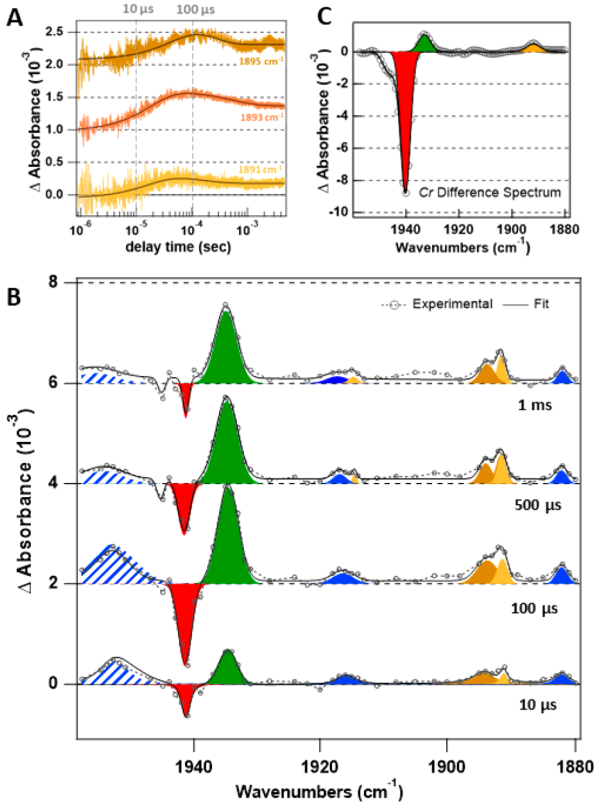

Figure 4. Potential jump TRIR spectra. (A) Potential jump IR transients at 1891, 1893, and 1895 cm^{-1}, offset for clarity. (B) TRIR spectra generated from IR transients, at time delays from 10 μs to 1 ms. The peaks are color coded as before; the blue shaded area >1950 cm^{-1} is due to overlapping bands of H_{red}−CO and $H_{sred}H^+$. (C) Steady-state difference FTIR spectrum of *Cr*HydA1 in the presence of photosensitizer and mediator, generated by subtracting the spectrum in the dark from the spectrum after continuous illumination.

The TRIR spectra have some features in common with the steady-state FTIR difference spectrum, including the bleach at 1941 cm^{-1} corresponding to loss of H_{ox} (red) and positive features corresponding to formation of reduced active-site intermediates, H_{red} (green), $H_{red}H^+$ (yellow), and $H_{sred}H^+$ (blue), although with different relative amplitudes. There are additional features in the TRIR spectra that are missing in the steady-state FTIR spectrum, highlighting the loss of information in steady state measurements of a dynamic system. The TRIR

DOI: 10.1021/jacs.9b08348
J. Am. Chem. Soc. 2019, 141, 16064−16070

spectrum never quite converges to the steady-state one, even after 10 ms, likely because diffusion of H_2 out of the illuminated volume is slower than 10 ms. In contrast, on the >10 s time scale of the steady state measurement, the illuminated volume equilibrates with the surrounding solution by slow diffusion of H_2.

A new feature at 1896 cm^{-1} (brown) emerges from these TRIR spectra. This feature is in close proximity to the peak near 1891 cm^{-1} that has been assigned previously to the $H_{red}H^+$ intermediate.[11] The resulting broad transient feature in this region was best fit to two overlapping Gaussian peaks at 1891 and 1896 cm^{-1}. These two bands persist over hundreds of μs, but the ratio of the amplitudes (1896/1891) decreases until >1 ms, when there are no longer two distinct populations. This observation is consistent with the transient nature of the 1896 cm^{-1} band, whereas some population of the $H_{red}H^+$ state remains in the steady-state spectrum. The new feature fits to a rise time of 49 μs and a decay time of 200 μs, distinct from the time response of the $H_{red}H^+$ absorbance at 1891 cm^{-1} as shown in Figure 4A. The distinct time-dependence of these bands further supports the conclusion that they arise from distinct species. The kinetics of this feature, together with its unique CO frequency, are consistent with a new intermediate state.

CONCLUSIONS

In this work, we have applied a laser-induced potential jump to initiate the catalytic cycle of the *Cr*HydA1 [FeFe] hydrogenase on a much faster time scale than the steady state turnover. Concurrent TRIR and TA spectroscopies enable the measurement of time-dependent flux through all known intermediate states. In summary, several important aspects of the catalytic mechanism emerge from these kinetics measurements:

(1) The rate of each one-electron reduction step is comparable to the rate of ET from the mediator to the enzyme. The interconversion rates between one-electron intermediate states induced by the potential jump do not appear to be proton limited at pH 8.4. Apparently, PT is fast enough to not be rate limiting, implying a rate of $\sim 10^{12}$ M^{-1} s^{-1} at pH 8.4, on the upper end of what has been observed in proteins.[38]

(2) All of the observed intermediates are kinetically competent to be part of the catalytic cycle. Their formation and decay rates are well within the previously determined turnover rate of the enzyme (TOF: 450 s^{-1}).[8] Further work will be required to measure the pH-dependent flux through each state as the enzyme cycles, in order to establish the major (and possibly minor) pathway(s). Nevertheless, it is difficult to reconcile the present results with the simpler catalytic schemes (a and b) presented in Figure 1, since we observe population flux through all of the major intermediated states as the enzyme turns over. For some intermediates we observe clear correlations between loss of one and gain of the other, indicating sequential transitions ($H_{ox} \rightarrow H_{red}$, $H_{red}H^+$; $H_{sred}H^+ \rightarrow H_{hyd}$). These observations are most consistent with mechanism c in Figure 1, although we cannot rule out the simpler mechanisms without pH- and isotope-dependent kinetics.

(3) The rate-limiting step of catalysis is not the interconversion of any of the known intermediate states. We detect rapid intermolecular ET and production of H_{red}, $H_{red}H^+$, $H_{sred}H^+$, and H_{hyd} within 100 μs. The slowest step (reformation of H_{ox} at the end of the catalytic cycle) occurs with a lifetime of 900 μs and the disappearance of H_{hyd} has a similar lifetime, meaning the chemical steps of the catalytic cycle are complete within the turnover lifetime measured in steady state (~1.1 ms). It is reasonable to conclude that the rate-determining step of the steady state process is not any of the chemical steps but instead involves H_2 release from the protein.

(4) A new intermediate state is observed with a CO frequency of 1896 cm^{-1}. While it is tempting to assign the new species to the H_2 bound state prior to reformation of the H_{ox} state, the CO frequency is very close to that of the $H_{red}H^+$ state, suggesting it has a similar electronic structure, possibly a form with a slightly different structure around the H-cluster. Characterization of the complete spectrum of this intermediate (including the CN modes) and calculations will be necessary to assign it to a proposed structure.

In summary, this work represents the first detailed study of the subturnover kinetics of all of the known intermediate states of an [FeFe] hydrogenase. We have established the kinetic relevance of all non-CO inhibited intermediates, an important step toward the development of a comprehensive catalytic model for [FeFe] hydrogenases.

ASSOCIATED CONTENT

Supporting Information

The Supporting Information is available free of charge on the ACS Publications website at DOI: 10.1021/jacs.9b08348.

Detailed experimental procedures, etc. (PDF)

AUTHOR INFORMATION

Corresponding Authors

*E-mail: briandyer@emory.edu.
*E-mail: james.birrell@cec.mpg.de.
*E-mail: wolfgang.lubitz@cec.mpg.de.

ORCID

Edward Reijerse: 0000-0001-9605-4510
James A. Birrell: 0000-0002-0939-0573
Wolfgang Lubitz: 0000-0001-7059-5327
R. Brian Dyer: 0000-0002-0090-7580

Notes

The authors declare no competing financial interest.

ACKNOWLEDGMENTS

The authors thank Nina Breuer for assistance with enzyme preparation, Tabea Mussfeldt for preparation of $[2Fe]^{ADT}$ complex, and Dr. Patricia Rodríguez Maciá for critically reading the manuscript. This work was supported by the U.S. National Science Foundation (CHE1807865 and DMR1808288) and the Max Planck Society.

REFERENCES

(1) Lubitz, W.; Ogata, H.; Rüdiger, O.; Reijerse, E. Hydrogenases. *Chem. Rev.* **2014**, *114*, 4081−4148.

(2) Ahmed, M. E.; Dey, S.; Darensbourg, M. Y.; Dey, A. Oxygen-Tolerant H2 Production by [FeFe]-H2ase Active Site Mimics Aided by Second Sphere Proton Shuttle. *J. Am. Chem. Soc.* **2018**, *140*, 12457−12468.

(3) Sommer, C.; Richers, C. P.; Lubitz, W.; Rauchfuss, T. B.; Reijerse, E. J. A [RuRu] Analogue of an [FeFe]-Hydrogenase Traps the Key

DOI: 10.1021/jacs.9b08348
J. Am. Chem. Soc. 2019, 141, 16064−16070

Hydride Intermediate of the Catalytic Cycle. *Angew. Chem.* **2018**, *130*, 5527−5530.
(4) Liu, T.; Darensbourg, M. Y. A Mixed-Valent, Fe(II)Fe(I), Diiron Complex Reproduces the Unique Rotated State of the [FeFe]-Hydrogenase Active Site. *J. Am. Chem. Soc.* **2007**, *129*, 7008−7009.
(5) Slater, J. W.; Marguet, S. C.; Monaco, H. A.; Shafaat, H. S. Going beyond Structure: Nickel-Substituted Rubredoxin as a Mechanistic Model for the [NiFe] Hydrogenases. *J. Am. Chem. Soc.* **2018**, *140*, 10250−10262.
(6) Onoda, A.; Hayashi, T. Artificial hydrogenase: biomimetic approaches controlling active molecular catalysts. *Curr. Opin. Chem. Biol.* **2015**, *25*, 133−140.
(7) Roy, S.; Groy, T. L.; Jones, A. K. Biomimetic model for [FeFe]-hydrogenase: asymmetrically disubstituted diiron complex with a redox-active 2,2'-bipyridyl ligand. *Dalton Transactions* **2013**, *42*, 3843−3853.
(8) Siebel, J. F.; Adamska-Venkatesh, A.; Weber, K.; Rumpel, S.; Reijerse, E.; Lubitz, W. Hybrid [FeFe]-Hydrogenases with Modified Active Sites Show Remarkable Residual Enzymatic Activity. *Biochemistry* **2015**, *54*, 1474−1483.
(9) Schilter, D.; Camara, J. M.; Huynh, M. T.; Hammes-Schiffer, S.; Rauchfuss, T. B. Hydrogenase Enzymes and Their Synthetic Models: The Role of Metal Hydrides. *Chem. Rev.* **2016**, *116*, 8693−8749.
(10) Wittkamp, F.; Senger, M.; Stripp, S. T.; Apfel, U. P. [FeFe]-Hydrogenases: recent developments and future perspectives. *Chem. Commun.* **2018**, *54*, 5934−5942.
(11) Sommer, C.; Adamska-Venkatesh, A.; Pawlak, K.; Birrell, J. A.; Rüdiger, O.; Reijerse, E. J.; Lubitz, W. Proton Coupled Electronic Rearrangement within the H-Cluster as an Essential Step in the Catalytic Cycle of [FeFe] Hydrogenases. *J. Am. Chem. Soc.* **2017**, *139*, 1440−1443.
(12) Rodríguez-Maciá, P.; Kertess, L.; Burnik, J.; Birrell, J. A.; Hofmann, E.; Lubitz, W.; Happe, T.; Rüdiger, O. His-Ligation to the [4Fe-4S] Subcluster Tunes the Catalytic Bias of [FeFe] Hydrogenase. *J. Am. Chem. Soc.* **2019**, *141*, 472−481.
(13) Haumann, M.; Stripp, S. T. The Molecular Proceedings of Biological Hydrogen Turnover. *Acc. Chem. Res.* **2018**, *51*, 1755−1763.
(14) Duan, J.; Senger, M.; Esselborn, J.; Engelbrecht, V.; Wittkamp, F.; Apfel, U.-P.; Hofmann, E.; Stripp, S. T.; Happe, T.; Winkler, M. Crystallographic and spectroscopic assignment of the proton transfer pathway in [FeFe]-hydrogenases. *Nat. Commun.* **2018**, *9*, 4726.
(15) Ratzloff, M. W.; Artz, J. H.; Mulder, D. W.; Collins, R. T.; Furtak, T. E.; King, P. W. CO-Bridged H-Cluster Intermediates in the Catalytic Mechanism of [FeFe]-Hydrogenase CaI. *J. Am. Chem. Soc.* **2018**, *140*, 7623−7628.
(16) Adamska-Venkatesh, A.; Krawietz, D.; Siebel, J.; Weber, K.; Happe, T.; Reijerse, E.; Lubitz, W. New Redox States Observed in [FeFe] Hydrogenases Reveal Redox Coupling Within the H-Cluster. *J. Am. Chem. Soc.* **2014**, *136*, 11339−11346.
(17) Senger, M.; Mebs, S.; Duan, J.; Shulenina, O.; Laun, K.; Kertess, L.; Wittkamp, F.; Apfel, U.-P.; Happe, T.; Winkler, M.; Haumann, M.; Stripp, S. T. Protonation/reduction dynamics at the [4Fe-4S] cluster of the hydrogen-forming cofactor in [FeFe]-hydrogenases. *Phys. Chem. Chem. Phys.* **2018**, *20*, 3128−3140.
(18) Greene, B. L.; Schut, G. J.; Adams, M. W. W.; Dyer, R. B. Pre-Steady-State Kinetics of Catalytic Intermediates of an [FeFe]-Hydrogenase. *ACS Catal.* **2017**, *7*, 2145−2150.
(19) Greene, B. L.; Vansuch, G. E.; Chica, B. C.; Adams, M. W. W.; Dyer, R. B. Applications of Photogating and Time Resolved Spectroscopy to Mechanistic Studies of Hydrogenases. *Acc. Chem. Res.* **2017**, *50*, 2718−2726.
(20) Berggren, G.; Adamska, A.; Lambertz, C.; Simmons, T. R.; Esselborn, J.; Atta, M.; Gambarelli, S.; Mouesca, J. M.; Reijerse, E.; Lubitz, W.; Happe, T.; Artero, V.; Fontecave, M. Biomimetic assembly and activation of [FeFe]-hydrogenases. *Nature* **2013**, *499*, 66.
(21) Davis, C. M.; Reddish, M. J.; Dyer, R. B. Dual time-resolved temperature-jump fluorescence and infrared spectroscopy for the study of fast protein dynamics. *Spectrochim. Acta, Part A* **2017**, *178*, 185−191.
(22) Greene, B. L.; Joseph, C. A.; Maroney, M. J.; Dyer, R. B. Direct Evidence of Active-Site Reduction and Photodriven Catalysis in Sensitized Hydrogenase Assemblies. *J. Am. Chem. Soc.* **2012**, *134*, 11108−11111.
(23) Greene, B. L.; Wu, C.-H.; McTernan, P. M.; Adams, M. W. W.; Dyer, R. B. Proton-Coupled Electron Transfer Dynamics in the Catalytic Mechanism of a [NiFe]-Hydrogenase. *J. Am. Chem. Soc.* **2015**, *137*, 4558−4566.
(24) Sanchez, M. L. K.; Wu, C.-H.; Adams, M. W. W.; Dyer, R. B. Optimizing electron transfer from CdSe QDs to hydrogenase for photocatalytic H_2 production. *Chem. Commun.* **2019**, *55*, 5579−5582.
(25) Mulder, D. W.; Boyd, E. S.; Sarma, R.; Lange, R. K.; Endrizzi, J. A.; Broderick, J. B.; Peters, J. W. Stepwise [FeFe]-hydrogenase H-cluster assembly revealed in the structure of HydAΔEFG. *Nature* **2010**, *465*, 248.
(26) Chica, B.; Wu, C.-H.; Liu, Y.; Adams, M. W. W.; Lian, T.; Dyer, R. B. Balancing electron transfer rate and driving force for efficient photocatalytic hydrogen production in CdSe/CdS nanorod-[NiFe] hydrogenase assemblies. *Energy Environ. Sci.* **2017**, *10*, 2245−2255.
(27) Zhao, F.; Li, Q.; Han, K.; Lian, T. Mechanism of Efficient Viologen Radical Generation by Ultrafast Electron Transfer from CdS Quantum Dots. *J. Phys. Chem. C* **2018**, *122*, 17136−17142.
(28) Sensi, M.; Baffert, C.; Fradale, L.; Gauquelin, C.; Soucaille, P.; Meynial-Salles, I.; Bottin, H.; de Gioia, L.; Bruschi, M.; Fourmond, V.; Léger, C.; Bertini, L. Photoinhibition of FeFe Hydrogenase. *ACS Catal.* **2017**, *7*, 7378−7387.
(29) Roseboom, W.; De Lacey, A. L.; Fernandez, V. M.; Hatchikian, E. C.; Albracht, S. P. J. The active site of the [FeFe]-hydrogenase from Desulfovibrio desulfuricans. II. Redox properties, light sensitivity and CO-ligand exchange as observed by infrared spectroscopy. *J. Biol. Inorg. Chem.* **2006**, *11*, 102−118.
(30) Albracht, S. P. J.; Roseboom, W.; Hatchikian, E. C. The active site of the [FeFe]-hydrogenase from Desulfovibrio desulfuricans. I. Light sensitivity and magnetic hyperfine interactions as observed by electron paramagnetic resonance. *J. Biol. Inorg. Chem.* **2006**, *11*, 88−101.
(31) Rodríguez-Maciá, P.; Birrell, J. A.; Lubitz, W.; Rüdiger, O. Electrochemical Investigations on the Inactivation of the [FeFe] Hydrogenase from Desulfovibrio desulfuricans by O2 or Light under Hydrogen-Producing Conditions. *ChemPlusChem* **2017**, *82*, 540−545.
(32) Goldet, G.; Brandmayr, C.; Stripp, S. T.; Happe, T.; Cavazza, C.; Fontecilla-Camps, J. C.; Armstrong, F. A. Electrochemical Kinetic Investigations of the Reactions of [FeFe]-Hydrogenases with Carbon Monoxide and Oxygen: Comparing the Importance of Gas Tunnels and Active-Site Electronic/Redox Effects. *J. Am. Chem. Soc.* **2009**, *131*, 14979−14989.
(33) Baffert, C.; Bertini, L.; Lautier, T.; Greco, C.; Sybirna, K.; Ezanno, P.; Etienne, E.; Soucaille, P.; Bertrand, P.; Bottin, H.; Meynial-Salles, I.; De Gioia, L.; Léger, C. CO Disrupts the Reduced H-Cluster of FeFe Hydrogenase. A Combined DFT and Protein Film Voltammetry Study. *J. Am. Chem. Soc.* **2011**, *133*, 2096−2099.
(34) Lemon, B. J.; Peters, J. W. Binding of Exogenously Added Carbon Monoxide at the Active Site of the Iron-Only Hydrogenase (CpI) from Clostridium pasteurianum. *Biochemistry* **1999**, *38*, 12969−12973.
(35) Talapin, D. V.; Koeppe, R.; Götzinger, S.; Kornowski, A.; Lupton, J. M.; Rogach, A. L.; Benson, O.; Feldmann, J.; Weller, H. Highly Emissive Colloidal CdSe/CdS Heterostructures of Mixed Dimensionality. *Nano Lett.* **2003**, *3*, 1677−1681.
(36) Rodríguez-Maciá, P.; Pawlak, K.; Rüdiger, O.; Reijerse, E. J.; Lubitz, W.; Birrell, J. A. Intercluster Redox Coupling Influences Protonation at the H-cluster in [FeFe] Hydrogenases. *J. Am. Chem. Soc.* **2017**, *139*, 15122−15134.
(37) Mulder, D. W.; Ratzloff, M. W.; Shepard, E. M.; Byer, A. S.; Noone, S. M.; Peters, J. W.; Broderick, J. B.; King, P. W. EPR and FTIR Analysis of the Mechanism of H2 Activation by [FeFe]-Hydrogenase HydA1 from Chlamydomonas reinhardtii. *J. Am. Chem. Soc.* **2013**, *135*, 6921−6929.
(38) Jeong, B. S.; Dyer, R. B. Proton Transport Mechanism of M2 Proton Channel Studied by Laser-Induced pH Jump. *J. Am. Chem. Soc.* **2017**, *139*, 6621−6628.

DOI: 10.1021/jacs.9b08348
J. Am. Chem. Soc. 2019, 141, 16064−16070